



Received September 09, 2024; accepted April 04, 2025; Date of publication April 15, 2025.  
The review of this paper was arranged by Associate Editor Roberto F. Coelho and Editor-in-Chief Telles B. Lazzarin

Digital Object Identifier <http://doi.org/10.18618/REP.e202532>

# Modified rainflow algorithm for temperature-time-dependent counting in lifetime estimation of power devices

Renata O. de Sousa<sup>1,\*</sup>, Rodrigo C. de Barros<sup>2</sup>, William C. S. Amorim<sup>3</sup>,  
Allan F. Cupertino<sup>4</sup>, Heverton A. Pereira<sup>5</sup>, Lenin M. F. Morais<sup>6</sup>

<sup>1</sup>Universidade Tecnológica Federal do Paraná, Department of Electronics, Curitiba – PR, Brazil.

<sup>2</sup>Universidade Federal de Ouro Preto, Departamento de Engenharia Elétrica, João Monlevade – MG, Brazil.

<sup>3</sup>Federal Institute of Education, Science, and Technology of Minas Gerais, Campus Itabirito, Itabirito – MG, Brazil.

<sup>4</sup>Universidade Federal de Juiz de Fora, Department of Electrical Energy, Juiz de Fora – MG, Brazil.

<sup>5</sup>Universidade Federal de Viçosa, Departamento de Engenharia Elétrica, Viçosa – MG, Brazil.

<sup>6</sup>Universidade Federal de Minas Gerais, Department of Electronics, Belo Horizonte – MG, Brazil.

e-mail: renatasousa@utfpr.edu.br\*; rodrigo.barros@ufpb.edu.br; william.amorim@ifmg.edu.br;  
allan.cupertino@ufjf.br; heverton.pereira@ufv.br; lenin@cpdee.ufmg.br

\*Corresponding author.

## ABSTRACT

Power electronic systems include many fragile elements, with power devices being the most prone to failure. Cycle counting algorithms are essential to evaluate power devices degradation and system reliability. Among the available options, the rainflow algorithm is the most widely used. Since the rainflow algorithm was originally designed for fatigue analysis, it faces challenges when applied to power devices. Specifically, the conventional rainflow algorithm cannot compute the effective heating time and the time-dependent equivalent mean temperature of the thermal cycles. Additionally, it counts cooling half-cycles, which contradicts the basis of lifetime models, as these models rely on data associated with heating temperature gradients. To address these limitations, this work introduces a modified rainflow algorithm for cycle counting in the lifetime estimation of power devices. This methodology enhances the conventional rainflow by enabling the calculation of effective heating time and mean temperature while also filtering out cooling half-cycles. The results demonstrate that the modified rainflow algorithm significantly affects the lifetime predictions for all critical joints in an IGBT module, regardless of the mission profile. Across all case studies, the utilization of the modified rainflow algorithm resulted in a damage reduction exceeding 53%.

**KEYWORDS** cycle counting algorithm, modified rainflow, lifetime estimation, power devices, reliability.

## I. INTRODUCTION

Since the electrification of modern society continues to advance rapidly, the electrical power system must expand continuously to meet the growing energy demands. A significant portion of this expansion is driven by power electronics technology, which enables the efficient control of power flow [1], [2]. In this context, ensuring reliable operation is essential for any power electronics system, since even a single component failure can result in significant maintenance costs and operational downtime. However, power electronic systems are composed of several fragile elements, including power semiconductor devices, capacitors, magnetics, controllers, sensors, and auxiliary devices. Among these elements, the power devices are the most susceptible to failure [3].

Wear-out failure of a device can be predicted to some extent if the degradation mechanisms are well understood. Consequently, the lifetime of a power electronic system can be extended by employing design and/or control techniques aimed at reducing wear-out of power devices [4]. Since power devices consist of various materials, thermal

cycling induces thermomechanical stress in their joints. This stress causes deformations that gradually lead to damage accumulation and, ultimately, result in the failure of critical joints, such as solders and bondwires [4]. Moreover, the shear stress-strain response of these joints to periodic thermal cycling forms stress-strain hysteresis loops. On this basis, the degradation of the critical joint material, as estimated by lifetime models, is directly related to the area enclosed by these hysteresis loops [4].

Lifetime estimation can be categorized into two types of thermal cycling: short-term and long-term [5]. Short-term analysis focuses on thermal stress caused by the grid fundamental frequency during the power converter's operation, while long-term analysis focuses on thermal stress caused by the mission profile variations [5]. The thermal cycling in short-term analyses is already well-defined due to the regularity of grid frequency. In contrast, the long-term thermal cycling exhibits irregular and unpredictable behavior driven by mission profile dynamics [6]–[8]. However, lifetime models are typically designed for constant conditions [4], [9]. Most models are based on power cycling

tests, in which power devices are actively heated by losses in the semiconductor and cooled again with the aid of cooling equipment [10]. Moreover, the temperature cycle is generally defined by the mean temperature ( $T_{[j,c]m}$ ), temperature swing ( $\Delta T_{j,c}$ ) and heating time ( $t_{on}$ ), as exemplified for a thermal cycle in Fig. 1. For this reason, a cycle counting algorithm is required to compute the hysteresis loops based on regular data series of  $T_{[j,c]m}$ ,  $\Delta T_{j,c}$  and  $t_{on}$ , enabling assessment of damage accumulation under variable thermal cycling conditions [6].

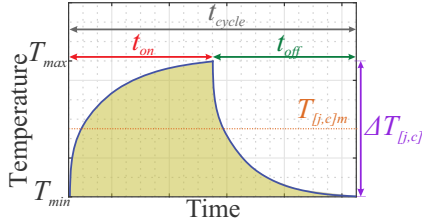


FIGURE 1. Example of thermal cycle.

The literature describes several cycle counting methods, such as half-cycle peak through counting, maximum edge peak through counting, rising edge peak through counting, and rainflow counting [11], [12]. Among these, rainflow cycle counting is the most widely used for power devices, since it results in lower error [12]. This method is based on the principle of treating hysteresis loops of a variable amplitude loading as equivalent cycles of constant amplitude loading [13].

The original rainflow algorithm was first proposed by M. Matsuishi and T. Endo in 1968 [14] to count full and half-cycles in strain-time signals for fatigue failure analysis in mechanical engineering. Due to this origin, rainflow counting presents challenges when implemented to real-time operating (online) damage assessment and/or when employed for lifetime estimation of power devices [4], [15]. Specifically, rainflow counting requires the complete time history (past and future) of the variable amplitude loading. This requirement poses a significant obstacle in estimating the remaining useful life of a power device during its operation. In practice, it would necessitate an indefinite amount of memory for online fatigue calculations. Some works proposed strategies to solve this issue, such as optimized algorithms, preset of the amplitude range and maximum time window [15]–[18]. Online rainflow application is beyond the scope of this work.

Several algorithms have been developed to implement rainflow counting [19]. One of the most widely referenced and utilized algorithms was created by Downing and Socie in 1982 [20]. This algorithm, based on a three-point rainflow counting rule [20], was later incorporated into ASTM E1049-85 as a standard practice for cycle counting in fatigue analysis [11]. Sandia National Laboratories implement the rainflow procedure employing the three-point counting rule with equivalent data information for fatigue analysis in wind turbine components [21]. In 2009, a rainflow function was

written by Nieslony [22] to be used in the MATLAB software environment. This function was written according to the ASTM standard and made available for download in MATLAB Central [22]. More recently, since MATLAB 2017b version, a rainflow function following ASTM standards is available directly on the software environment.

Conventional rainflow algorithms do not adequately consider the temperature-time-dependence crucial for the lifetime estimation of power devices [23], [24]. These algorithms often compute the mean temperatures independent of cycle time. Nevertheless, the stress induced by temperature is inherently time-dependent in power devices [23], [25].

The heating time significantly influences damage accumulation in power devices [24], [26], as exemplified in the lifetime curves of an ABB HiPak IGBT in Fig.2 (a) and (b) for  $t_{on} = 1$  s and  $t_{on} = 60$  s. However, conventional rainflow computes the time only at the maximum and minimum temperature points ( $T_{max}$  and  $T_{min}$ ). While some approaches approximate heating time as half of the cycle time ( $t_{cycle}$ ) derived from the rainflow function, this assumption relies on the premise of equal heating and cooling time ( $t_{off}$ ), which may not always hold true [27].

The rainflow algorithm counts all half-cycles of the data. Nevertheless, most lifetime models are based on power cycling tests, in which only the heating process is actively controlled [9], [10]. Consequently, these lifetime models consider only heating transients. As discussed in reference [24], only half-cycles representing heating transients should be considered for lifetime estimation of power devices.

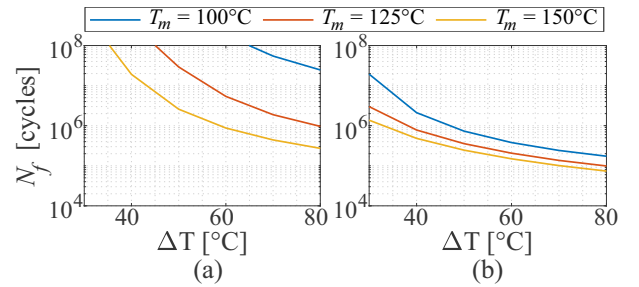


FIGURE 2. Power cycling lifetime model of chip solder of ABB HiPak IGBT as a function of  $T_{jm}$ ,  $\Delta T_j$  for: (a)  $t_{on} = 1$  s; (b)  $t_{on} = 60$  s [9].

Reference [26] proposed a methodology for cycle counting in the lifetime estimation of power devices: the modified rainflow algorithm. The methodology adapts the three-point rainflow algorithm (conventional rainflow) available in MATLAB environment to a four-point rainflow algorithm (modified rainflow) [25]. The modified rainflow algorithm is capable of computing the effective heating time and the effective mean temperature while filtering out cooling half-cycles counted with the conventional rainflow. However, this algorithm also filters all heating half-cycles except for the last one.

This work extends the methodology presented in [26]. The new version of the modified rainflow algorithm, while

still adapting the conventional MATLAB rainflow to a four-point algorithm to compute the effective heating time and mean temperature, now also eliminates only cooling half-cycles, preserving all heating half-cycles. Thus, the modified rainflow aims to extract from the temperature profiles the parameters that characterize the thermal cycling and which are consistent with the parameters that should be used as input in the lifetime models. The impact of this refined methodology on lifetime estimation is evaluated using different mission profiles. Moreover, the modified rainflow function is available for download in [28]. A general lifetime estimation procedure applicable to any power converter application is presented. Finally, the impact of the modified rainflow algorithm is compared to conventional rainflow in terms of damage accumulation, system-level reliability, and processing time.

This paper is organized as follows. Section II introduces the long-term lifetime estimation and reliability procedure for power devices. Section III introduces the proposed modified rainflow algorithm. The case studies are described in Section IV. In Section V, the obtained results are presents. Ultimately, Section VI presents the conclusions of this work.

## II. LIFETIME ESTIMATION OF POWER DEVICES

Fig. 3 illustrates the long-term lifetime estimation procedure. Real-world mission profiles, representative of the operational conditions of the power converter in the field, are used. The power device losses ( $P$ ) are determined using a power loss model based on the operating conditions of the power converter. A thermal model is then used to estimate the junction ( $T_j$ ) and case ( $T_c$ ) temperature profiles of the power devices.

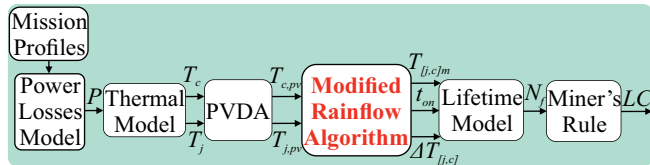


FIGURE 3. Long-term lifetime estimation procedure.

To employ lifetime models, the profile data must be prepared appropriately. This requires a cycle counting algorithm for thermal cycling classification [4]. The modified rainflow algorithm proposed in this work is used for this purpose. This algorithm flowchart is presented in Fig. 4 and detailed in Section III.

To compute hysteresis loops, the modified rainflow algorithm should be applied only to the extreme points (peaks and valleys) of the temperatures. Therefore, the temperature data was preprocessed using a peaks and valleys detection algorithm (PVDA). This results in a filtered temperature dataset containing only peak and valley information ( $T_{j,pv}$  and  $T_{c,pv}$ ) [23]. Subsequently, the modified rainflow algorithm is applied to this filtered data. This yields a regular

data series containing  $T_{[j,c]m}$ ,  $\Delta T_{j,c}$  and  $t_{on}$ . Thereafter, the regular temperature data is applied to the lifetime model.

The lifetime of a power module is limited by the mechanical fatigue of the package. This fatigue arises from thermally induced mechanical stress caused by disparities in thermal expansion coefficients among the constituent materials. Since power devices incorporate materials with varying thermal expansion coefficients, these materials are constrained from freely expanding. This constraint results in thermally induced mechanical stress within critical joints of the power device, such as base plate and conductor solders (BPCS), bondwires (BW), and chip solders (CS) [29]. These joints are placed in different locations within the power module. Thus, each lifetime model considers the temperature of the location of its respective joint.

Finally, the power device life consumption ( $LC$ ) can be accumulated using the Miner's rule [30], as follows:

$$LC = \sum_k \frac{n_k}{N_{f,k}}, \quad (1)$$

where  $n_k$  is the  $k^{th}$  number of repeated cycles obtained from the modified rainflow algorithm,  $N_{f,k}$  is the  $k^{th}$  number of cycles to failure, and  $LC$  is the life consumption for each critical joints of each power device in the converter.

To approximate the results of practical applications, Monte Carlo simulations with a population of 10,000 samples are carried out for each power device and respective critical joint, using the respective lifetime model [31], [32]. Subsequently, the unreliability function of each joint is obtained from its respective lifetime distribution and combined to compute the system-level unreliability [33]. The power device critical joints unreliability curves are computed and combined following the methodology described in [31], [32]. Moreover, the unreliability function indicates the proportion of the failure population over time. Therefore, this is an important figure of merit to evaluate the probability of failure over time of the entire converter (system-level).

## III. MODIFIED RAINFLOW ALGORITHM

Conventional rainflow algorithms are unable to determine the effective heating time and the time-dependent effective mean temperature. In essence, these algorithms only identify the time instances at the temperature extremes: the initial cycle ( $t_i$ ) and the final cycle ( $t_f$ ). These points are exemplified in Fig. 5 (a) and (b) for descending and ascending cycles, respectively. Although some approaches, such as those that utilize the MATLAB rainflow function developed by A. Nieslony [22], approximate the heating time as half of the cycle time, this assumption relies on the premise of equal cooling and heating times, which may not always hold true [27], as illustrated in Fig. 5 (a). Even with the newest MATLAB rainflow function introduced in MATLAB version R2017b [34], only  $t_i$  and  $t_f$  are explicitly computed.

Furthermore, the stress-strain hysteresis loop is temperature-time-dependent [23]. As verified in

reference [35], the stress that metals can withstand decreases as the temperature increases. For this reason, reference [25] proposed a four-point algorithm for conservative damage estimation. This work demonstrated that for temperatures below the threshold temperature of metals (usually  $< 250^\circ\text{C}$ ) a time-dependent equation should be employed to compute an equivalent mean temperature of the stress-strain hysteresis loop. Since most power devices operate with a maximum rated temperature lower than  $175^\circ\text{C}$ , the time-dependent equivalent mean temperature should be considered in the lifetime estimation. As exemplified in Table 1 and Table 2, the temperature values computed considering the simple mean temperature calculation of conventional rainflow and the equivalent temperature calculation can differ. Consequently, since the lifetime of power devices is highly sensitive to temperature, even minor discrepancies in temperature calculations, especially when accumulated over numerous data points, can significantly affect the lifetime estimation results.

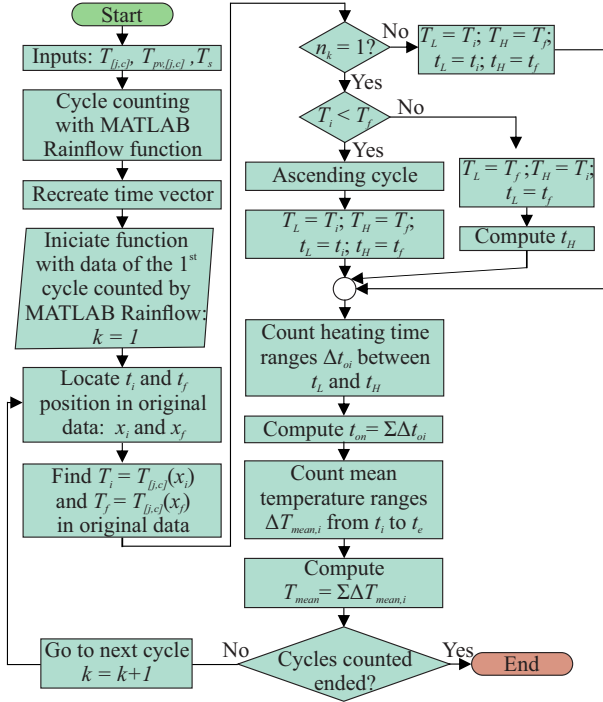


FIGURE 4. Flowchart of modified rainflow algorithm.

To solve these issues, the modified rainflow algorithm is proposed. The flowchart of the modified rainflow algorithm is exhibited in Fig. 4. The modified rainflow algorithm adapts the three-point rainflow algorithm (conventional rainflow) available in the MATLAB environment to a four-point rainflow counting capable of computing the effective heating time and effective mean temperature while simultaneously filtering out cooling half-cycles.

As observed in Fig. 4,  $t_i$  and  $t_f$ , resulting from the MATLAB rainflow function, are used to identify the corresponding thermal cycle within the original data and to

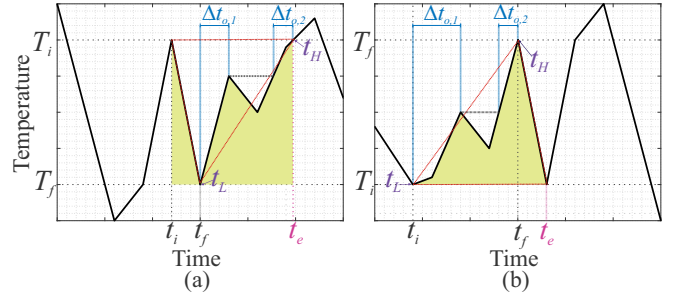


FIGURE 5. Modified rainflow algorithm counting for: (a) descending cycle; (b) ascending cycle.

determine its direction. Based on the respective temperatures at  $t_i$  ( $T_i$ ) and  $t_f$  ( $T_f$ ), the cycle is classified. If  $T_i > T_f$ , the cycle counted by MATLAB rainflow function is descending (Fig. 5 (a)). Otherwise, if  $T_i < T_f$ , the cycle that was counted is ascending (Fig. 5 (b)).

Furthermore,  $t_e$  represents the time at which the thermal cycle is fully completed, defined in [23]:

$$t_e = \frac{T_i - T_{be}}{T_{af} - T_{be}} (t_{af} - t_{be}) + t_{be}, \quad (2)$$

where  $t_{be}$  and  $T_{be}$  are the time and temperature, respectively, in the original data at the point immediately preceding the end of the thermal cycle. Similarly,  $t_{af}$  denotes the time in the original data at the point immediately following the end of the thermal cycle.

This verification defines  $t_L$  as the time of the lowest temperature, in which the heating starts in the thermal cycle, and  $t_H$  as the time of the highest temperature, in which the heating ends. If  $T_i > T_f$ ,  $t_L = t_f$  and  $t_H = t_e$ . Otherwise, if  $T_i < T_f$ ,  $t_L = t_i$  and  $t_H = t_f$ .

Subsequently, the heating time intervals ( $\Delta t_{o,j}$ ) between  $t_L$  and  $t_H$ , are calculated and summed to determine the effective heating time ( $t_{on} = \sum_j \Delta t_{o,j}$ ).

The equivalent mean temperature is calculated by considering each time interval within the original data (with sample time  $T_s$ ) that falls within the full thermal cycle (from  $t_i$  to  $t_e$ ). For each interval, the mean temperature is calculated and then weighted by the proportion of the duration of the interval to the total cycle time ( $t_e - t_i$ ), as described in [23]:

$$\Delta T_{mean,j} = \frac{T_2 - T_1}{2} \frac{t_2 - t_1}{t_e - t_i}, \quad (3)$$

where  $t_1$  and  $T_1$  represent the time and temperature, respectively, in the original data at the beginning of the interval.  $t_2$  and  $T_2$  represent the time and temperature, respectively, in the original data at the end of the interval. Subsequently, the equivalent mean temperature values within each interval ( $\Delta T_{mean,j}$ ) between  $t_i$  and  $t_e$  are computed and summed to determine the effective mean temperature ( $T_{mean} = \sum_j \Delta T_{mean,j}$ ).

To demonstrate the proposed algorithm, conventional and modified rainflows are applied to the temperature profile of Fig. 6. The conventional rainflow output and modified

rainflow output are presented in Table 1 and Table 2, respectively, for this temperature profile.

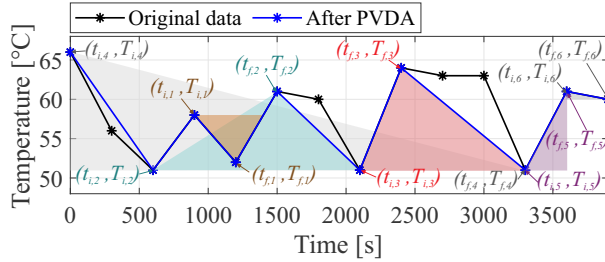


FIGURE 6. Example for a temperature profile.

For the temperature profile of Fig. 6, two half-cycles ( $k = 4$  and  $k = 6$ ) are filtered/eliminated by modified rainflow, as indicated in Table 2 as non-counted (n.c.). These half-cycles present cooling transients that should not be considered in the lifetime estimation of power devices. The half-cycle ( $k = 5$ ) presenting heating transient is counted by modified rainflow since should be considered in the lifetime estimation. Regarding the  $\Delta T_j$ , the values computed by conventional rainflow are maintained after modified rainflow implementation, since the modified rainflow does not affect this parameter. On the other hand,  $t_{on}$  and  $T_{j,m}$  obtained from modified rainflow differ from conventional rainflow, since the effective  $t_{on}$  and  $T_{j,m}$  are computed by the modified rainflow algorithm.

TABLE 1. Conventional rainflow output and respective  $t_{on}$  computed.

$k$	$n_k$	$T_{j,m}$ [°C]	$\Delta T_j$ [°C]	$t_i$ [s]	$t_f$ [s]	$t_{on}$ [s]
1	1	55.0	6	900	1200	300
2	1	56.0	10	600	1500	900
3	1	57.5	13	2100	2400	300
4	0.5	58.5	15	0	3300	3300
5	0.5	56.0	10	3300	3600	300
6	0.5	60.5	1	3600	3900	300

TABLE 2. Modified rainflow output.

$k$	$n_k$	$T_{j,m}$ [°C]	$\Delta T_j$ [°C]	$t_{on}$ [s]
1	1	55.0	6	200
2	1	56.4	10	400
3	1	60.2	13	300
4	0.5	n.c.	n.c.	n.c.
5	0.5	56.0	10	300
6	0.5	n.c.	n.c.	n.c.

\* n.c. indicates the non-counted cycles.

#### IV. CASE STUDY

The performance of the modified rainflow algorithm is evaluated within the context of a modular multilevel converter-based static synchronous compensator (MMC-STATCOM) application. The MMC-STATCOM topology is illustrated in

Fig. 7. This topology comprises  $N$  submodules (SMs) per arm. Each SM incorporates a capacitor bank represented by the equivalent capacitance ( $C$ ) and four power devices ( $S_1$ ,  $S_2$ ,  $D_1$  and  $D_2$ ). In this work, the MMC-STATCOM design and control strategy follows the same approach of [32]. MMC-STATCOM main parameters are presented in Table 3. In addition, ABB HiPak IGBT modules, part number 5SND0800M170100, rated at 1.7 kV and 800A, are considered.

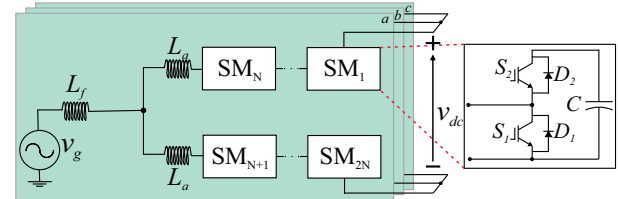


FIGURE 7. MMC-STATCOM topology with half-bridge SMs.

TABLE 3. Parameters of the MMC-STATCOM.

Parameter	Value
SMs per arm ( $N$ )	21
dc-link voltage ( $v_{dc}$ )	21.61 kV
Rated power ( $S_n$ )	17 MVA
Line-to-line rms grid voltage ( $V_g$ )	13.8 kV
Grid frequency ( $f_g$ )	60 Hz
Switching frequency ( $f_{sw}$ )	200 Hz
SM capacitance ( $C$ )	14 mF
Capacitors in parallel per SM	7
Transformer inductance ( $L_f$ )	1.5 mH
Arm inductance ( $L_a$ )	2.97 mH

Wear-out analyses are performed using simulations implemented within the MATLAB/Simulink and PLECS software environments. The simulations were performed on a Dell Inspiron i15-3583-AS100P computer equipped with an Intel Core i7-8565U CPU (1.80 GHz), an AMD Radeon 520 dedicated graphics card, and 8 GB of RAM.

The mission profiles were derived from measurements collected over a year in locations within Southeastern Brazil, with a sampling rate of  $T_s = 5$  min. Fig. 8 (a) depicts the ambient temperature ( $T_a$ ) mission profile. Furthermore, two distinct reactive power ( $q$ ) mission profiles are utilized, as shown in Fig. 8 (b) and (c) for case studies 1 and 2, respectively. In Case 1 (Fig. 8 (b)), a seasonal variation in the reactive power is observed, characterized by a decrease in reactive power injection during the middle of the year. Besides,  $q$  exhibits both positive and negative values, indicating both lagging and leading reactive power operation, respectively. In Case 2 (Fig. 8 (c)),  $q$  demonstrates an oscillatory pattern throughout the year and exclusively exhibits positive values, signifying solely leading reactive power operation.

The power losses model is performed by look-up tables derived from the curves provided in the ABB HiPak IGBT module datasheet, considering a defined set of operational

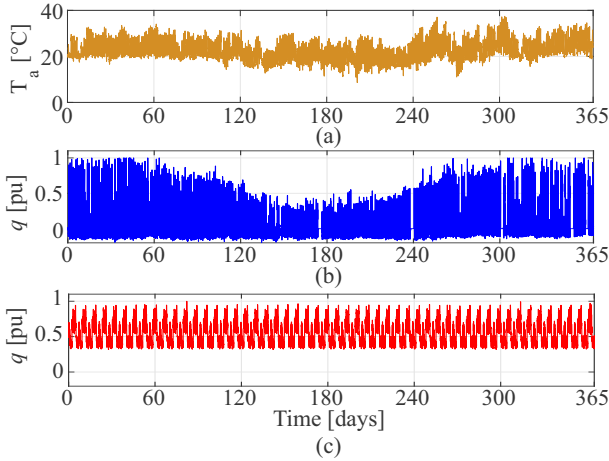


FIGURE 8. Mission profiles: (a) ambient temperature; (b) reactive power - Case 1; (c) reactive power - Case 2.

conditions. Moreover, the Foster thermal model [36] with a single heatsink per SM is employed. The heatsink thermal impedance is designed to ensure that the case temperature remains below 80°C, adhering to the upper limit of temperature specified in the lifetime models [9], [37].

Lifetime models, also based on look-up tables provided by ABB for HiPak IGBT modules [9], are utilized. All critical joints within the power module, including base plate and conductor solders (BPCS), chip solder (CS), and bondwires (BW), are considered. Each lifetime model incorporates the temperature to its respective joint location. Notably, the BW lifetime model exhibits negligible dependence on heating time. This observation is consistent with advancements in ABB HiPak technology, which have resulted in bond wire performance being minimally impacted by heating time [9]. Consequently, the inputs of each lifetime model are:  $T_{c,m}$ ,  $\Delta T_c$  and  $t_{on}$  for BPCS;  $T_{j,m}$ ,  $\Delta T_j$  and  $t_{on}$  for CS; and  $T_{j,m}$  and  $\Delta T_{j,c}$  for BW.

The lifetime models provided by ABB are based on power cycling experiments with a maximum heating time of 16 h. Therefore, it is assumed that viscoplastic deformation saturates for heating time exceeding 16 h [38].

## V. RESULTS

The results for Case 1 and Case 2 are presented in the following subsections. These results are based on the methodology described in Section II (detailed in [32]) and Section III.

### A. Case 1

Fig. 9 shows the case and junction temperature profile of the diode  $D_1$ . In this case study,  $D_1$  emerges as the most critically stressed power device within the submodule, exhibiting the highest average temperatures throughout the year ( $T_{c,avg} = 25.79^\circ\text{C}$  and  $T_{j,avg} = 26.08^\circ\text{C}$ ). Furthermore, this device also experiences the most significant maximum temperature variations throughout the year ( $\Delta T_{c,max} = 70.56^\circ\text{C}$  and  $\Delta T_{j,max} = 74.68^\circ\text{C}$ ). As observed in Fig. 9, the

temperature profiles closely mirror the shape of the reactive power mission profile, characterized by lower temperatures during the middle of the year.

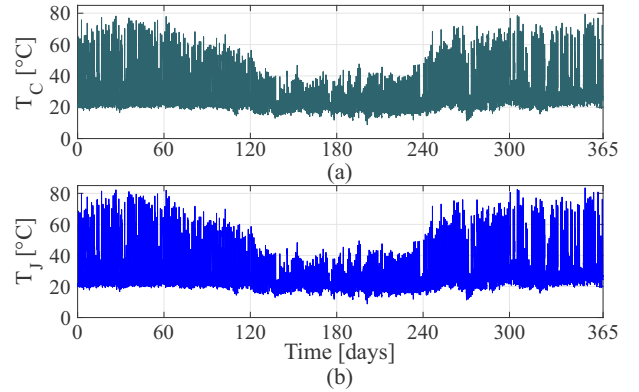


FIGURE 9. Case 1 profiles of: (a) case temperature; (b) junction temperature.

Fig. 10 shows a comparison of the modified and conventional rainflow of the first 10 thermal cycles counted. As presented in Fig. 10 (a), the mean temperature counted by conventional and modified rainflow can exhibit discrepancies. For these 10 cycles, the percentage mean temperature difference achieves  $\Delta T_{diff,max} = 0.4\%$ . This discrepancy highlights the significance of considering the time-dependence of temperature within the cycle counting process. Fig. 10 (b) demonstrates that the effective heating time computed using modified rainflow differs significantly from the approximation obtained by simply assuming  $t_{on} = t_f - t_i$  in conventional rainflow. For these 10 cycles, the percentage heating time difference achieves  $\Delta t_{diff,max} = 82.0\%$ . This result underscores the importance of calculating the effective heating time.

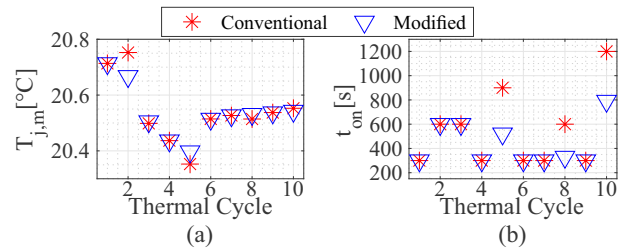


FIGURE 10. Modified and conventional rainflows data of the 10 first thermal cycles: (a) mean temperature; (b) heating time.

Fig. 11 shows the junction temperature histograms for modified and conventional rainflows. A similar distribution is observed for both rainflows. At the data point with the highest cycle count, the mean temperature is identical for both counting methods. However,  $t_{on}$  decreased by approximately 73.7% when using the modified rainflow at this extreme point. This finding demonstrates the significant influence of the modified rainflow algorithm on heating time estimation for this mission profile. Moreover, conventional rainflow and modified rainflow computed 26,150 and 26,143

thermal cycles, respectively. This difference in the number of cycles indicated that the modified rainflow algorithm filtered 7 cooling half-cycles which should not be considered in the life computation.

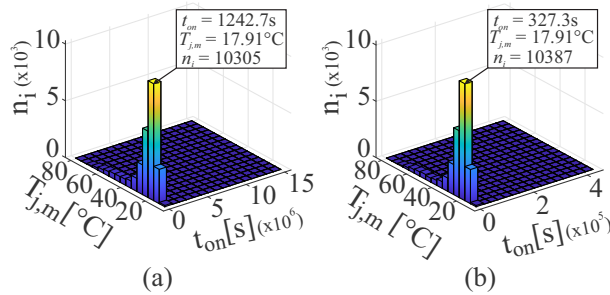


FIGURE 11. Case 1 histogram of: (a) conventional rainflow; (b) modified rainflow.

Fig. 12 shows the static damage  $LC$  for all critical joints of the power devices, calculated using both modified and conventional rainflow methods. For  $D_1$ , the modified rainflow resulted in a substantial reduction in  $LC$  for BPCS, CS, and BW by approximately 52%, 72%, and 53%, respectively. These results demonstrate the significant impact of the modified rainflow algorithm on lifetime estimations of all critical joints within the power devices. Notably, even the bondwire lifetime, which is unaffected by the heating time, is influenced by the modified rainflow due to the computation of the effective mean temperature and filtering of cooling half-cycles.

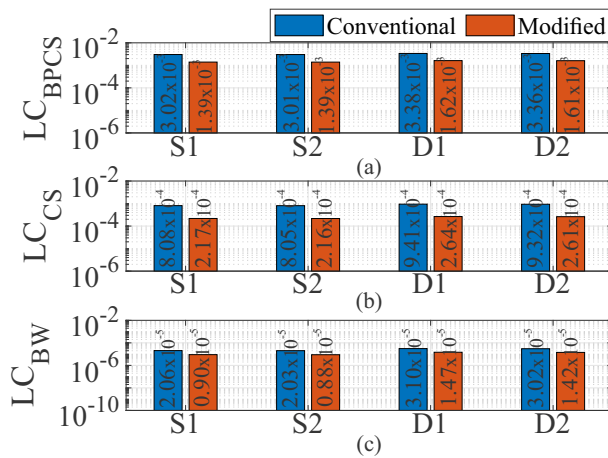


FIGURE 12. Case 1 static damages of: (a) base plate and conductor solders – BPCS; (b) chip solder – CS; (c) bondwire – BW.

Fig. 13 presents the processing time required from the PVDA output until the damage computation with Miner's Rule with conventional and modified rainflow. The error bars represent one standard deviation of uncertainty considering 10 executions. As observed in Fig. 13, the modified rainflow algorithm increased, on average, the processing time of the damage computation by 14.7 s. Nevertheless, part of the error bars of conventional and modified rainflows intercept each

other. This indicates a small probability that the processing time of the modified rainflow is the same or lower than the conventional rainflow. This will depend on the computer processing speed during the procedure, which can vary due to other applications running in parallel.

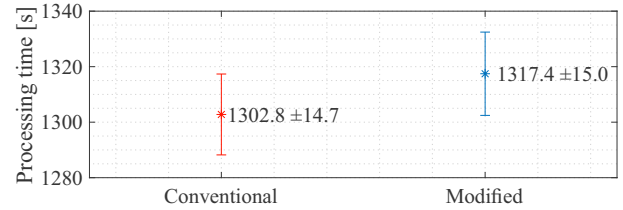


FIGURE 13. Processing time of the damage computation with each counting algorithm of Case 1.

Fig. 14 exhibits the MMC-STATCOM unreliability at system-level, considering all power device critical joints. The time at which 10% of the samples fail ( $B_{10}$  lifetime approach) is highlighted. As observed, the unreliability is higher when computed using conventional rainflow. Moreover,  $B_{10}$  is 56.2% lower with modified rainflow. This is a consequence of the higher damage accumulation computed with the conventional rainflow algorithm.

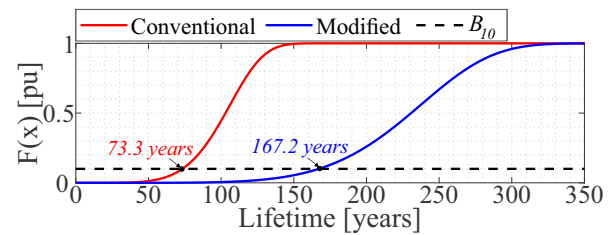


FIGURE 14. Unreliability function at system-level for Case 1.

## B. Case 2

Fig. 15 shows the case and temperature profile of the diode  $D_1$ . In this case study,  $D_1$  emerges as the most critically stressed power device within the submodule, exhibiting the highest average temperatures throughout the year ( $T_{c,avg} = 45.12^\circ\text{C}$  and  $T_{j,avg} = 47.11^\circ\text{C}$ ). Furthermore,  $D_1$  experiences the most significant maximum temperature variations throughout the year ( $\Delta T_{c,max} = 53.64^\circ\text{C}$  and  $\Delta T_{j,max} = 56.33^\circ\text{C}$ ). As observed in Fig. 15, the temperature profiles closely mirror the oscillatory pattern of the reactive power mission profile throughout the year. In particular, this case study demonstrates a more severe operating environment compared to Case 1, characterized by higher average temperatures.

Fig. 16 shows a comparison of the modified and conventional rainflow data for the first 10 thermal cycles counted. As presented in Fig. 16 (a), the mean temperature calculated by modified and conventional rainflow methods can exhibit discrepancies. For these 10 cycles, the percentage mean temperature difference achieves approximately  $\Delta T_{diff,max} =$

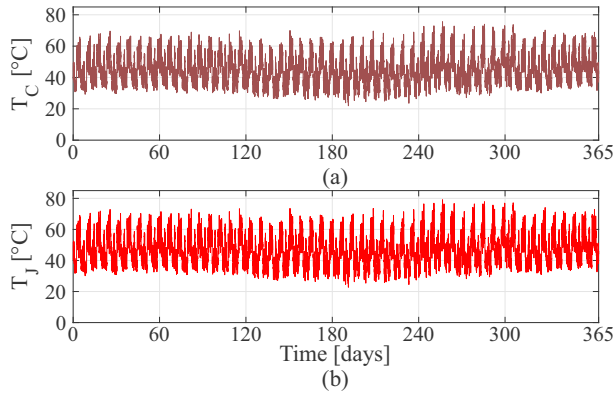


FIGURE 15. Case 2 profile of: (a) case temperature; (b) junction temperature.

1%. For Fig. 16 (b), the heating time computed using modified and conventional rainflow were found to be identical ( $\Delta t_{diff,max} = 0\%$ ). This indicates that the 10 first cycles are ascending cycles.

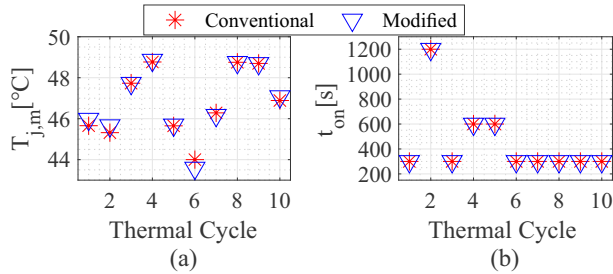


FIGURE 16. Conventional and modified rainflows information of the 10 first thermal cycles: (a) mean temperature; (b) heating time.

Fig. 17 shows the junction temperature histograms for modified and conventional rainflows. A similar distribution is observed for both rainflows. At the data point with the highest cycle count, the mean temperature exhibits a minor difference of  $0.01^{\circ}\text{C}$  between the rainflows. However,  $t_{on}$  decreases by approximately 61.5% when using the modified rainflow approach at this extreme point. This finding demonstrates the significant influence of the modified rainflow algorithm on heating time estimation for this mission profile. Moreover, conventional rainflow and modified rainflow computed 25,008 and 24,997 thermal cycles, respectively. This difference in the number of cycles indicated that the modified rainflow algorithm filtered 11 cooling half-cycles, which should not be considered in the life computation.

Fig. 18 shows the static damage  $LC$  for all critical joints of the power devices, computed using modified and conventional rainflows. For  $D_1$  The modified rainflow approach resulted in a substantial reduction in  $LC$  for BPCS (52%), CS (69%), and BW (53%), respectively. These results demonstrate the significant impact of the modified rainflow algorithm on lifetime estimation for all critical joints within power devices. Notably, even the bondwire lifetime, which is unaffected by heating time, was influenced by the modified

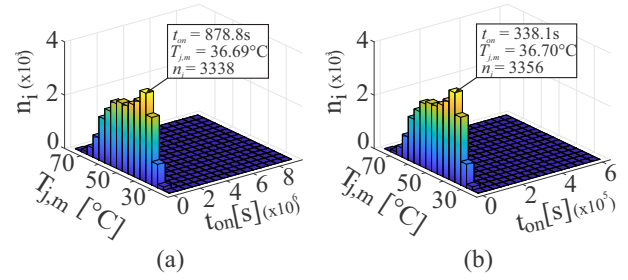


FIGURE 17. Histogram of Case 2 of: (a) conventional rainflow; (b) modified rainflow.

rainflow method due to the computation of the effective mean temperature and the filtering of cooling half-cycles.

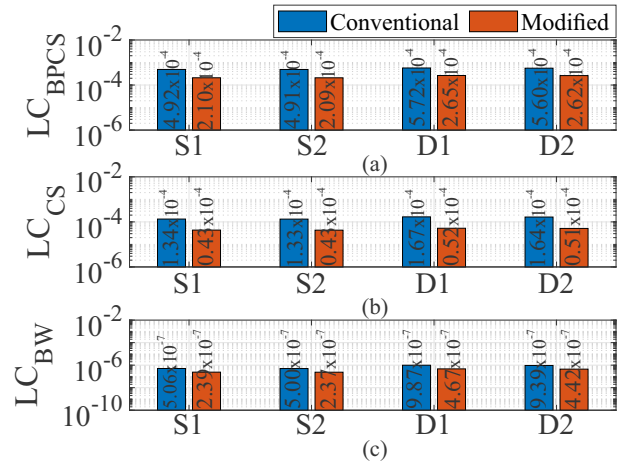


FIGURE 18. Case 2 static damages of: (a) base plate and conductor solders – BPCS; (b) chip solder – CS; (c) bondwire – BW.

Fig. 19 presents the processing time required from the PVDA output until the damage computation with Miner’s Rule with conventional and modified rainflow. The error bars represent one standard deviation of uncertainty considering 10 executions. As observed in Fig. 19, the modified rainflow algorithm increased, on average, the processing time of the damage computation by 69.4 s. Unlike in Case 1, part of the error bars of conventional and modified rainflows do not intercept each other.

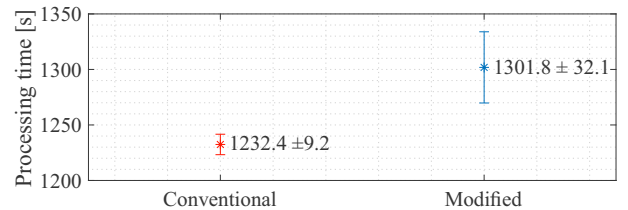


FIGURE 19. Processing time of the damage computation with conventional and modified rainflows of Case 2.

Fig. 20 exhibits the MMC-STATCOM unreliability at system-level, considering all power devices critical joints. The time at which 10% of the samples fail ( $B_{10}$  lifetime approach) is highlighted. As observed, the unreliability is

higher when computed using conventional rainflow. Moreover,  $B_{10}$  is 56.6% lower with modified rainflow. This is a consequence of the higher damage accumulation computed with the conventional rainflow algorithm.

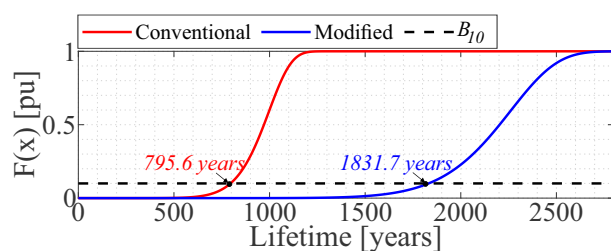


FIGURE 20. Unreliability function at system-level for Case 2.

### C. Modified rainflow effect on different mission profiles

Table 4 summarizes the main results of the case studies to evaluate the effect of modified rainflow applied to cases with distinct mission profiles. The reactive power mission profile exhibits seasonality, with reduced injection around mid-year, whereas Case 2 displays an oscillatory pattern throughout the year. Consequently, Case 1 and Case 2 exhibit the highest maximum temperature variation and average temperature over the year, respectively. According to [33], maximum temperature variation and the average temperature of the profile correlate with life consumption. These parameters are directly linked to  $T_{[j,c]m}$  and  $\Delta T_{j,c}$ , respectively, which serve as inputs for power device lifetime models.

TABLE 4. Summary of the main results of Case 1 and Case 2.

Parameter	Case 1	Case 2
Seasonality over the year	yes	no
$T_{c,avg}$ [ $^{\circ}$ C]	25.79	45.12
$T_{j,avg}$ [ $^{\circ}$ C]	26.08	47.11
$\Delta T_{c,max}$ [ $^{\circ}$ C]	70.56	53.64
$\Delta T_{j,max}$ [ $^{\circ}$ C]	74.68	56.33
$\Delta T_{diff,max}$ for the 1 <sup>st</sup> 10 cycles	0.4%	1%
$\Delta t_{diff,max}$ for the 1 <sup>st</sup> 10 cycles	82.0%	0%
Cooling half-cycles filtered	7	11
Increased processing time [s]	14.7	69.4
$LC_{BPFS}$ reduction with MR <sup>1</sup>	52%	54%
$LC_{CS}$ reduction with MR <sup>1</sup>	72%	69%
$LC_{BW}$ reduction with MR <sup>1</sup>	53%	53%
$B_{10}$ reduction with MR <sup>1</sup>	56.2%	56.6%

<sup>1</sup>MR means modified rainflow.

For the first 10 thermal cycles counted, the maximum difference between the mean temperatures ( $\Delta T_{diff,max}$ ) remains comparable for both cases. However, the maximum difference between the heating times ( $\Delta t_{diff,max}$ ) for Case 1 is significantly higher than for Case 2. These findings indicate that the modified rainflow method can exhibit varying impacts depending on the specific characteristics of the mission profile. The histograms of Fig. 11 and Fig.

17 reveal that the application of modified rainflow has a less pronounced effect on the mean temperature distribution for both case studies, while exerts higher influence on the heating time computation. As shown for the extreme point highlighted in the histograms,  $t_{on}$  can decrease 73.7% and 61.5% for Case 1 and Case 2, respectively. As presented in Table 4, both cases exhibit a comparable number of filtered cooling half-cycles and increased processing time when employing modified rainflow.

As observed in Table 4, the modified rainflow demonstrates a similar percentage effect on the estimation of the life consumption for the critical joints and the system-level unreliability (highlighted for  $B_{10}$  lifetime). Moreover, the 53% reduction in  $LC_{BW}$  underscores that the calculation of the effective mean temperature and the cooling half-cycles filtering of modified rainflow significantly influence lifetime estimation.

## VI. CONCLUSIONS

This work introduces a modified rainflow algorithm for the lifetime estimation of power devices. This methodology adapts the conventional rainflow by incorporating the features of filtering cooling half-cycles and computing the effective heating time and effective mean temperature. According to the literature, these modifications allow to extract from the temperature profiles the parameters that characterize the thermal cycling and which are consistent with the parameters that should be used as input in the lifetime models. The impact of the modified rainflow algorithm on life consumption was assessed using an MMC-STATCOM and two case studies with distinct reactive power mission profiles.

The results demonstrate a more pronounced effect of the modified rainflow on the heating time computation, as evidenced by the temperature distributions, where  $t_{on}$  decreases 73.7% and 61.5% for Case 1 and Case 2, respectively. Although the amount of cooling half-cycle filtering is inherently linked to the dynamics of the mission profile, both cases exhibited a comparable level of filtering. Furthermore, the impact of modified rainflow on processing time was minimal, remaining below 6% for both case studies.

Furthermore, this methodology exerts a substantial influence on the lifetime estimation of all critical joints within the power devices for both case studies. A reduction exceeding 53% in static damage is observed for all critical joints across both case studies when employing modified rainflow. Notably, even the lifetime estimation of bondwires, which are unaffected by the heating time, was influenced by modified rainflow due to the computation of effective mean temperature and the filtering of cooling half-cycles.

The modified rainflow function is readily available for download in [28]. For future developments of this work, the investigation of the modified rainflow algorithm considering different converter applications and power devices (i.e., blocking voltages and manufacturers) is an interesting topic.

Experimental verification using accelerated testing will be considered for future work.

## ACKNOWLEDGMENT

The authors are grateful for the financial support provided by the P&D project ANEEL/CEMIG D0727, CNPq (Conselho Nacional de Desenvolvimento Científico e Tecnológico) - projects 311056/2020-2, 408058/2021-8 and 307172/2022-8 and FAPEMIG (Fundação de Amparo à Pesquisa do Estado de Minas Gerais) - project RED-00216-23. In addition, this work was carried out with the support of the CAPES (Coordenação de Aperfeiçoamento de Pessoal de Nível Superior) - Financing Code 001.

## AUTHOR'S CONTRIBUTIONS

**R.O.SOUSA:** Conceptualization, Data Curation, Formal Analysis, Investigation, Methodology, Project Administration, Validation, Visualization, Writing – Original Draft, Writing – Review & Editing. **R.C.BARROS:** Conceptualization, Data Curation, Formal Analysis, Investigation, Methodology, Validation, Visualization, Writing – Original Draft, Writing – Review & Editing. **W.C.S.AMORIM:** Conceptualization, Data Curation, Formal Analysis, Investigation, Methodology, Visualization. **A.F.CUPERTINO:** Conceptualization, Data Curation, Formal Analysis, Funding Acquisition, Investigation, Methodology, Project Administration, Resources, Supervision, Validation, Visualization. **H.A.PEREIRA:** Conceptualization, Data Curation, Formal Analysis, Funding Acquisition, Investigation, Methodology, Project Administration, Resources, Supervision, Validation, Visualization. **L.M.F.MORAIS:** Conceptualization, Data Curation, Formal Analysis, Investigation, Methodology, Project Administration, Supervision, Validation, Visualization.

## PLAGIARISM POLICY

This article was submitted to the similarity system provided by Crossref and powered by iThenticate – Similarity Check.

## REFERENCES

- [1] D. Tan, "Power Electronics: Historical Notes, Recent Advances And Contemporary Challenges", *Eletrônica de Potência*, vol. 25, no. 4, p. 386–394, Dec. 2020, doi:10.18618/REP.2020.4.00701.
- [2] F. Blaabjerg, H. Wang, I. Vernica, B. Liu, P. Davari, "Reliability of Power Electronic Syst. for EV/HEV Applications", *Proc of the IEEE*, vol. 109, no. 6, pp. 1060–1076, 2021, doi:10.1109/JPROC.2020.3031041.
- [3] J. Falck, C. Felgmacher, A. Rojko, M. Liserre, P. Zacharias, "Reliability of Power Electronic Systems.: An Industry Perspective", *IEEE Ind Electron Magazine*, vol. 12, no. 2, pp. 24–35, 2018, doi:10.1109/MIE.2018.2825481.
- [4] H. S. H. Chung, H. Wang, F. Blaabjerg, M. Pechtt, *Reliability of Power Electronic Converter Systems*, IET, 2015, doi:10.1049/PBPO080E.
- [5] K. Ma, M. Liserre, F. Blaabjerg, T. Kerekes, "Thermal Loading and Lifetime Estimation for Power Device Considering Mission Profiles in Wind Power Converter", *IEEE Trans on Power Electron*, vol. 30, no. 2, pp. 590–602, 2015, doi:10.1109/TPEL.2014.2312335.
- [6] K. Ma, F. Blaabjerg, "Reliability-cost models for the power switching devices of wind power converters", in *IEEE Int. Symp. on Power Electron. for Distrib. Gener. Syst.*, pp. 820–827, 2012, doi:10.1109/PEDG.2012.6254096.
- [7] R. Silva, R. de Barros, W. Boaventura, A. Cupertino, H. Pereira, "Correction strategy for wear-out prediction of PV inverters considering the mission profile resolution effects", *Microelectronics Reliability*, vol. 135, p. 114605, 2022, doi:10.1016/j.microrel.2022.114605.
- [8] R. C. de Barros, W. do Couto Boaventura, H. A. Pereira, A. F. Cupertino, "Lifetime Evaluation of a Three-phase Photovoltaic Inverter During Harmonic Current Compensation", *Eletrônica de Potência*, vol. 27, no. 2, pp. 108–116, jun. 2022, doi:10.18618/REP.2022.2.0054.
- [9] ABB, *Application note, Load-cycling Capability of Hi-Pak IGBT Modules.*, 2014.
- [10] A. Wintrich, U. Nicolai, W. Tursky, T. Reimann, *Application Manual Power Semiconductors*, SEMIKRON, 2015.
- [11] ASTM International, *Standard Practices for Cycle Counting in Fatigue Analysis*, 2017.
- [12] K. Mainka, M. Thoben, O. Schilling, "Lifetime calculation for power modules, application and theory of models and counting methods", in *14th Eur. Conf. on Power Electron. and Appl.*, pp. 1–8, 2011.
- [13] R. Anthes, "Modified rainflow counting keeping the load sequence", *Int Journal of Fatigue*, vol. 19, no. 7, pp. 529–535, 1997, doi:https://doi.org/10.1016/S0142-1123(97)00078-9.
- [14] M. Matsuishi, T. Endo, "Fatigue of metals subjected to varying stress", *Japan Soc of Mechanical Engineers*, vol. 68, no. 2, pp. 37–40, 1968.
- [15] A. Antonopoulos, S. D'Arco, M. Hernes, D. Pefitsis, "Challenges and Strategies for a Real-Time Implementation of a Rainflow-Counting Algorithm for Fatigue Assessment of Power Modules", in *IEEE Appl. Power Electron. Conf. and Exposition*, pp. 2708–2713, 2019, doi:10.1109/APEC.2019.8722284.
- [16] U. H. Clormann, T. Seeger, "RAINFLOW-HCM - Ein Zählverfahren für Betriebsfestigkeitsnachweise auf werkstoffmechanischer Grundlage", *Stahlbau*, vol. 55, no. 3, pp. 65–71, 1986.
- [17] V. Samavatian, H. Iman-Eini, Y. Avenas, "An efficient online time-temperature-dependent creep-fatigue rainflow counting algorithm", *Int Journal of Fatigue*, vol. 116, pp. 284–292, 2018, doi:10.1016/j.ijfatigue.2018.06.037.
- [18] Z. Chen, F. Gao, C. Yang, T. Peng, L. Zhou, C. Yang, "Converter Lifetime Modeling Based on Online Rainflow Counting Algorithm", in *IEEE 28th Int. Symp. on Industrial Electron.*, pp. 1743–1748, 2019, doi:10.1109/ISIE.2019.8781196.
- [19] M. Musallam, C. M. Johnson, "An Efficient Implementation of the Rainflow Counting Algorithm for Life Consumption Estimation", *IEEE Trans on Reliability*, vol. 61, no. 4, pp. 978–986, 2012, doi:10.1109/TR.2012.2221040.
- [20] S. Downing, D. Socie, "Simple rainflow counting algorithms", *Int Journal of Fatigue*, vol. 4, no. 1, pp. 31–40, 1982, doi:https://doi.org/10.1016/0142-1123(82)90018-4.
- [21] L. Schluter, *Programmer's Guide for LIFE2's Rainflow Counting Algorithm Sandia Report*, Sandia National Laboratories, 1991.
- [22] A. Nieslony, "Rainflow Counting Algorithm", , 2003, Available in: <https://www.mathworks.com/matlabcentral/fileexchange/3026-rainflow-counting-algorithm>.
- [23] L. R. GopiReddy, L. M. Tolbert, B. Ozpineci, J. O. P. Pinto, "Rainflow Algorithm-Based Lifetime Estimation of Power Semiconductors in Utility Applications", *IEEE Trans on Ind Appl*, vol. 51, no. 4, pp. 3368–3375, 2015, doi:10.1109/TIA.2015.2407055.
- [24] A. Antonopoulos, S. D'Arco, M. Hernes, D. Pefitsis, "Limitations and Guidelines for Damage Estimation Based on Lifetime Models for High-Power IGBTs in Realistic Application Conditions", *IEEE Journal of Emerging and Sel Top in Power Electron*, vol. 9, no. 3, pp. 3598–3609, 2021, doi:10.1109/JESTPE.2020.3004093.
- [25] M. Nagode, M. Hack, "An online algorithm for temperature influenced fatigue life estimation: stress–life approach", *Int Journal of Fatigue*, vol. 26, no. 2, pp. 163–171, 2004, doi:10.1016/S0142-1123(03)00107-5.
- [26] R. O. De Sousa, R. C. De Barros, W. C. S. Amorim, A. F. Cupertino, H. A. Pereira, "Modified Rainflow Algorithm for Lifetime Estimation of Semiconductors Devices", in *IEEE 8th Southern Power Electron. Conf. and 17th Brazilian Power Electron. Conf.*, pp. 1–8, 2023, doi:10.1109/SPEC56436.2023.10408046.
- [27] F. Hosseinabadi, S. Chakraborty, S. K. Bhoi, G. Prochart, D. Hrvanovic, O. Hegazy, "A Comprehensive Overview of Reliability Assessment Strategies and Testing of Power Electronics Converters", *IEEE Open Journal of Power Electronics*, vol. 5, pp. 473–512, 2024, doi:10.1109/OJPEL.2024.3379294.

- [28] R. O. Sousa, “Repositorio GESEP - Gerência de Especialistas em Sistemas Elétricos de Potência”, Modified Rainflow Function - Version 02 (updated on June 26, 2024), 2024, Available in: <https://gesep.ufv.br/repositorio/>.
- [29] R. Kosiba, *Technical Explanation SEMIPACK*, SEMIKRON, 2018.
- [30] M. A. Miner, “Cumulative damage in fatigue”, *American Soc of Mechanical Engineers - J Appl Mechanics*, vol. 12, pp. 159–164, 1945, doi:10.1115/1.4009458.
- [31] P. D. Reigosa, H. Wang, Y. Yang, F. Blaabjerg, “Prediction of Bond Wire Fatigue of IGBTs in a PV Inverter Under a Long-Term Operation”, *IEEE Trans on Power Electron*, vol. 31, no. 10, pp. 7171–7182, 2016, doi:10.1109/TPEL.2015.2509643.
- [32] R. O. d. Sousa, A. F. Cupertino, L. M. F. Morais, H. A. Pereira, R. Teodorescu, “Experimental Validation and Reliability Analyses of Minimum Voltage Control in Modular Multilevel Converter-Based STATCOM”, *IEEE Trans on Ind Electron*, pp. 1–10, 2023, doi:10.1109/TIE.2023.3303634.
- [33] R. de Sousa, A. Cupertino, L. Morais, H. Pereira, “Wear-out failure analysis of modular multilevel converter-based STATCOM: The role of the modulation strategy and IGBT blocking voltage”, *Microelectron Reliability*, vol. 128, p. 114426, 2022, doi:10.1016/j.microrel.2021.114426.
- [34] MATLAB, “Rainflow”, 2017, Available in: <https://www.mathworks.com/help/signal/ref/rainflow.html>.
- [35] X. Chen, L. Zhang, M. Sakane, H. Nose, “Tensile stress-strain curves modeling of four kinds of solders with temperature and rate dependence”, *Key Eng Mater*, vol. 297-300, p. 905–911, 2005, doi:10.4028/www.scientific.net/KEM.297-300.905.
- [36] Infineon, *Transient thermal measurements and thermal equivalent circuit models*, 2020.
- [37] P. Asimakopoulos, K. Papastergiou, T. Thiringer, M. Bongiorno, “Heat sink design considerations in medium power electronic applications with long power cycles”, in *17th Eur. Conf. on Power Electron. and Applications*, pp. 1–9, 2015, doi:10.1109/EPE.2015.7309150.
- [38] Infineon, *AN2019-05 - PC and TC Diagrams*, 2019.

## BIOGRAPHIES

**Renata Oliveira de Sousa** received the B.S. degree in electrical engineering from the Federal University of Viçosa, Viçosa, Brazil, in 2018, the M.S. degree in electrical engineering from the Federal Center for Technological Education of Minas Gerais, Belo Horizonte, Brazil, in 2019, and the Ph.D. degree in electrical engineering from the Federal University of Minas Gerais, Belo Horizonte, in 2022. From 2021 to 2022, she was a Guest Ph.D. student with the Department of Energy, Aalborg University, Aalborg, Denmark. From 2020 to 2021, she was an Adjunct Professor with the Department of Electrical Engineering, Federal Center for Technological Education of Minas Gerais. She is currently an Assistant Professor at the Department of Electronics, Federal University of Technology - Paraná, Curitiba, Brazil. She is a member of the Brazilian Power Electronics Society (SOBRAEP). Her main research interests include the reliability of power electronics-based systems, multilevel converters, smart battery-based storage systems, and systems developed in smart materials.

**Rodrigo Cássio de Barros** holds a degree in Electrical Engineering from the Federal University of Viçosa - UFV (2017), a sandwich degree in Electrical Engineering from the University of Minnesota - UofM (2014 - 2015). He holds a master's degree in Electrical Engineering from the Federal Center for Technological Education of Minas Gerais - CEFET (2018). Furthermore, he holds a PhD in Electrical Engineering from the Federal University of Minas Gerais UFMG (2019 - 2022). He worked as a substitute professor at CEFET-MG (Leopoldina Campus) and as Adjunct Professor A at the Center for Exact and Technological Sciences at the Federal University of Recôncavo da Bahia (UFRB). He is currently an Adjunct Professor A at Federal University of Ouro Preto (UFOP), João

Monlevade campus. He teaches subjects in the areas of Energy Conversion, Electrical Machines, and Power Electronics. He is currently also a Professor of the Specialization in Isolated and Grid-Connected Photovoltaic Systems at the Federal University of Viçosa. He is an aspiring member of the Brazilian Society of Power Electronics (SOBRAEP) and manager of GESEP (Management of Power Electronics Specialists). He has experience in the field of power electrical systems and power electronics, mainly working on the following topics: multifunctional inverters, reliability of photovoltaic inverters, harmonic current compensation, and energy storage systems.

**William Caires Silva Amorim** received the B.S. degree in electrical engineering from the Universidade Federal de Viçosa (UFV), Viçosa, Brazil, in 2018. He received the M.S. degree in electrical engineering from Federal Center for Technological Education of Minas Gerais, Belo Horizonte, Brazil, in 2019. In this institution, he carried out research in the area of information theory, with emphasis on Coding Theory by the PICME Program. He has been an EBTT Professor with the Campus Itabirito, IFMG, since 2022. He was a Substitute Professor with the Department of Electrical Engineering in UFV and a Researcher Assistant with Gerencia de Especialistas em Eletrônica de Potência (GESEP). His research interests include power electronics and electrical power systems, with focus in the modular multilevel cascade converters and BESS.

**Allan Fagner Cupertino** received the B.S. degree in electrical engineering from the Federal University of Viçosa (UFV) in 2013, the M.S. and Ph.D. degrees in Electrical Engineering from the Federal University of Minas Gerais (UFMG) in 2015 and 2019, respectively. He was a guest Ph.D. at the Department of Energy Technology, Aalborg University from 2018 to 2019. From 2014 to 2022, he was an Assistant Professor in the area of electric machines and power electronics at the Federal Center of Technological Education of Minas Gerais (CEFET). Since 2023, he has been with the Department of Electrical Energy at the Federal University of Juiz de Fora (UFJF). His main research interests include renewable energy conversion systems, smart battery energy storage systems, cascaded multilevel converters, and reliability of power electronics.

Prof. Cupertino was the recipient of the President Bernardes Silver Medal in 2013, the SOBRAEP Ph.D. Thesis Award in 2020 and the IAS CMD Ph.D. Thesis Contest in 2021. He is a member of the Brazilian Power Electronics Society (SOBRAEP) and the Brazilian Society of Automatics (SBA). In 2024, he became an IEEE Senior Member and researcher at the National Institute of Electrical Energy (INERGE).

**Heverton Augusto Pereira** received the B.S. degree in electrical engineering from the Federal University of Viçosa, Viçosa, Brazil, in 2007, the M.Sc. degree in electrical engineering from the University of Campinas, Campinas, Brazil, in 2009, and the Ph.D. degree in electrical engineering from the Federal University of Minas Gerais, Belo Horizonte, Brazil, in 2015. In 2014, he was a Visiting Researcher with the Department of Energy Technology, Aalborg University, Aalborg, Denmark. In 2009, he was with the Department of Electric Engineering, Federal University of Viçosa, where he is currently an Adjunct Professor. His research interests include grid-connected converters for photovoltaic systems, HVDC/FACTS, and drives based on modular multilevel converters.

**Lenin Martins Ferreira Morais** received the bachelor's degree, the master's degree, and the doctor's degree, all in electrical engineering from the Federal University of Minas Gerais, Belo Horizonte, Brazil, in 2000, 2002, and 2007, respectively. He is currently a Full Professor with the

Electronics Engineering Department, Federal University of Minas Gerais. He was a Postdoctoral Intern with the Laboratoire Plasma et Conversion d'Energie - LAPLACE, Université Toulouse III Paul Sabatier, Toulouse, France, and with the Institut de Recherche Technologique - IRT Saint Exupéry, Toulouse, France. He has experience in the field of electrical engineering, with emphasis on power electronics, industrial electronics, and electronic systems and controls. His research interests mainly include the following: projects of converters with high density of power/high perfor-

mance, electronic reactors for high intensity discharge lamps, power LEDs, circuits for power factor correction, repetitive control, control based on positivity, PWM methods, Electronic Transformer, ballast electronic, LED drivers, PFC circuits, repetitive control, passivity-based control, adaptive control, Solid State Transformer. Member of SOBRAEP (Brazilian Society of Power Electronics) since 2005. Member of IEEE Power Electronics Society. Member of IEEE Industrial Electronics Society.